Nanoscale Research Letters

NANO EXPRESS Open Access

Strain Tunable Bandgap and High Carrier Mobility in SiAs and $SiAs_2$ Monolayers from First-Principles Studies

Shouyan Bai[1], Chun-Yao Niu[1*], Weiyang Yu[2], Zhili Zhu[1], Xiaolin Cai[2] and Yu Jia[1,3*]

Abstract

Searching for new stable free-standing atomically thin two-dimensional (2D) materials is of great interest in the fundamental and practical aspects of contemporary material sciences. Recently, the synthesis of layered SiAs single crystals has been realized, which indicates that their few layer structure can be mechanically exfoliated. Performing a first-principles density functional theory calculations, we proposed two dynamically and thermodynamically stable semiconducting SiAs and $SiAs_2$ monolayers. Band structure calculation reveals that both of them exhibit indirect band gaps and an indirect to direct band even to metal transition are found by application of strain. Moreover, we find that SiAs and $SiAs_2$ monolayers possess much higher carrier mobility than MoS_2 and display anisotropic transportation like the black phosphorene, rendering them potential application in optoelectronics. Our works pave a new route at nanoscale for novel functionalities of optical devices.

Keywords: SiAs, Two-dimensional semiconductors, Higher carrier mobility, First-principles

Background

Atomically thin two-dimensional (2D) crystals have become one of the most rapidly burgeoning field of contemporary material science. The versatile electronic properties, excellent electron mobility, and promising applications in nanoelectronics and optoelectronics are driving a large percentage of condensed-matter physicists to hunt for new 2D materials. Following graphene [1–4], a huge number of other 2D materials have been synthesized such as silicene [5–7], boron-nitride nanosheets [8, 9], transition-metal dichalcogenides (TMDs) [10, 11], black phosphorus [12, 13], borophene [14–16], arsenene [17, 18], tellurene [19], and their isoelectronic compounds [20–23]. The list of 2D materials is fast expanding, and more than thousands kinds of such materials are now known, encompassing the full spectrum of electronic and other properties. And their novel properties , different from or even better than those of their bulk counterparts, are theoretically predicted and experimentally confirmed firmly.

Although extensive and substantial efforts were invested in finding diverse 2D materials including some that already possess bandgaps or other desirable properties, consensus has not been reached. Graphene with marvelous carrier mobility, high mechanical stability, and massless dirac electrons has attracted much attention to date, but the lacking of an intrinsic band gap hinder its application in modern electronic devices industry. Although large efforts have been made, opening up a sizeable band gap without side-effect has not been reached [24, 25]. TMDs with high performance in optoelectronic devices indeed have intrinsic band gap, but exhibit poor in carrier mobility [26–28]. Black and blue phosphorus with a strain sensitive tunable band gap and anisotropic high carrier mobility can not keep stable in air [13, 29]. Recently, the synthesis of layered SiAs and $SiAs_2$ single crystals has been realized [30–32], which indicates that few layer structure can be obtained by mechanically exfoliated.

In the present work, based on a first-principles density functional theory calculations (DFT), we proposed

*Correspondence: niuchunyao@zzu.edu.cn; jiayu@zzu.edu.cn
[1]International Laboratory for Quantum Functional Materials of Henan, Zhengzhou University, 450001 Zhengzhou, People's Republic of China
[3]Key Laboratory for Special Functional Materials of Ministry of Education, Henan University, 475001 Kaifeng, People's Republic of China
Full list of author information is available at the end of the article

two dynamically and thermodynamically stable semiconducting monolayers SiAs and $SiAs_2$. They both possess indirect band gaps (2.39 eV and 2.13 eV respectively). Application of isotropic strain along two in-plane directions practically transforms the SiAs ($SiAs_2$) monolayer into a direct-gap 1.75 eV (1.60 eV) material. Moreover, we find that SiAs and $SiAs_2$ monolayers possess much higher carrier mobility than MoS_2 and display anisotropic transportation like the black phosphorene, rendering them potential application in optoelectronics. Our works paves a new route at nanoscale for novel functionalities of optical devices.

Computational Methods

The DFT calculations are performed using Vienna ab initio simulation package (VASP) code [33]. We used the Perdew-Burke-Ernzerhof (PBE) [34] exchange-correlation functional under the generalized gradient approximation(GGA). The projector augmented wave (PAW) method [35] was employed to describe the electron-ion interaction. A vacuum of 20 Å perpendicular to the sheets (along the *c* axis) was applied to avoid the interaction between layers. A kinetic energy cut-off of 500 eV is used for the plane wave basis set. The Brillouin-zone sampling is carried out with a $15 \times 5 \times 1$ Monkhorst-Pack [36] grid for 2D sheets. Convergence criteria employed for both the electronic self-consistent relaxation and ionic relaxation are set to be 10^{-4} and 0.01 eV/Å for energy and force, respectively. The phonon calculations are carried out using the supercell method through the PHONOPY code [37, 38], and the real-space force constants of supercells are calculated in the density-functional perturbation theory (DFPT) as implemented in VASP. Moreover, a more strict energy (10^{-8} eV/atom) and force convergence criterion (10^{-4} eV/Å) are used during the vibrational spectra calculations. In the molecular dynamics(MD) calculations, ($3 \times 3 \times 1$) supercells are employed and the temperature is kept at 300 K for 6 ps with a time step of 2 fs in the moles-volume-temperature (NVT) ensemble. The raman spectra were calculated at the PBE level of theory using the CASTEP code [39–41].

Results and Discussions

The geometrical structures and electron density distribution of relaxed free-standing 2D SiAs and $SiAs_2$ are presented in Fig. 1a, b, respectively, and their bulk structures are shown in Additional file 1: Figure S1 of the supplementary material. As shown in Additional file 1: Figure S1a and b, the bulk SiAs($SiAs_2$) possesses C2/m(Pbam) symmetry and consists of stacked Si-As layers weakly bound by van der Waals forces with a distance of 3.06 Å (1.66 Å). The unit cell of monolayer SiAs is rhombic and its optimized crystal parameters are $a_1 = 3.69$Å and $b_1 = 10.83$Å with $\varphi = 99.81°$. SiAs contains 6 Si atoms and 6 As

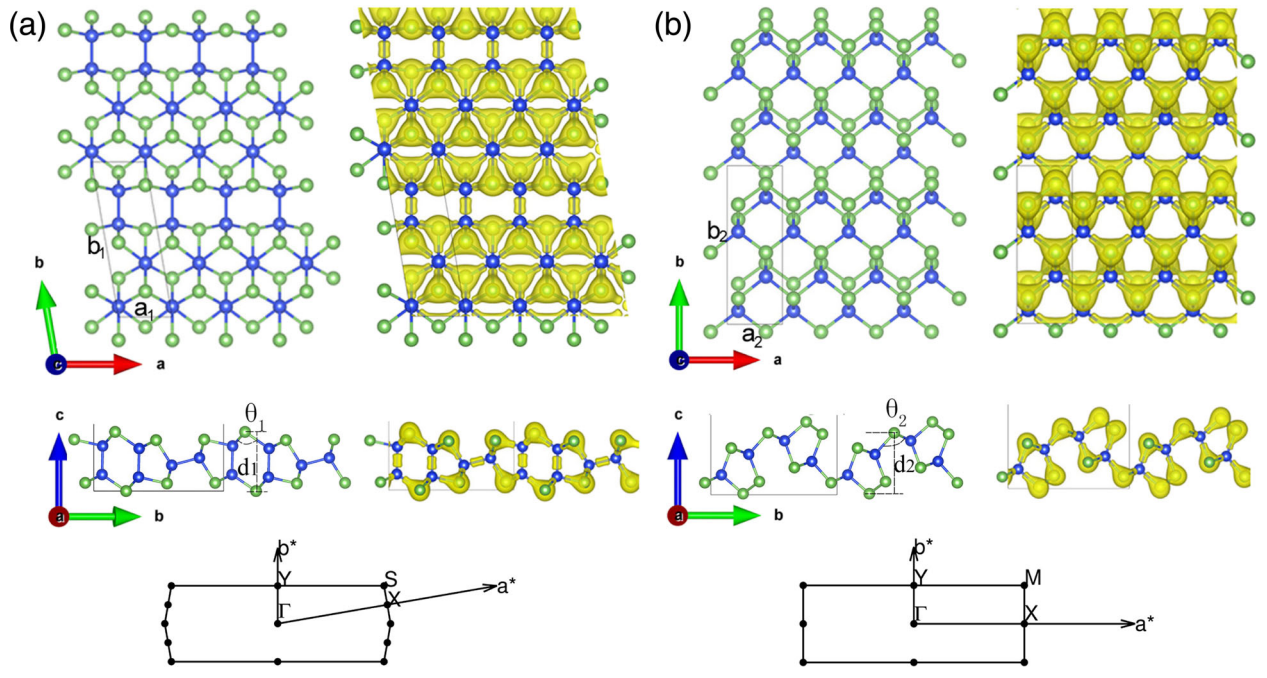

Fig. 1 Geometrical structure and electron density distribution of monolayers SiAs and $SiAs_2$. (Color online) Top and side views of monolayers **a** SiAs and **b** $SiAs_2$ geometrical structure and electron density distribution and the associated Brillouin zone. The blue and green ball indicate the Si and As atom, respectively

atoms. Each Si atom has four nearest neighboring atoms (3 As and 1 Si) while each As atom forms only three covalent bonds with neighboring Si atoms. It exists two kinds of bonds, namely, Si–Si and Si–As bonds. And the Si–Si bond length is about 2.35 Å and that of Si–As is in the range of 2.39 Å and 2.43 Å, and the buckled height is $d_1 = 4.86$ Å. At the side view of monolayer SiAs, a eyeglass-stringed like structure is formed with double and single layers alternately bulked. Another monolayer structure of silicon and arsenic compound is $SiAs_2$. Its prime cell contains 4 Si atoms and 8 As atoms, with a rectangular structure and the optimized crystal parameters are $a_2 = 3.68$Å and $b_2 = 10.57$ Å. Each As atoms has three nearest neighboring Si atoms or forms one covalent bond with neighboring Si atoms and two covalent bonds with themselves, while each Si atoms has only four nearest neighboring As atoms. Unlike the former, $SiAs_2$ owns weaker As–As bond (2.50 Å) instead of Si–Si bond. And its Si–As bonds range from 2.41 Å to 2.45 Å, and the buckled height is $d_2 = 5.09$ Å. From the electron density distribution, the As atoms attract electron from Si Atoms for their large electronegativity and have a larger electron density. In order to assist future experimental characterization, we further calculated and checked the Raman spectra of bulk and monolayer SiAs and $SiAs_2$. Clear shifts between the monolayer and the full crystals have been seen in Additional file 1: Figure S2 of the supplementary material, whose origins have been identified as the influence of layers van der Waals interaction [42].

To learn the stability of SiAs ($SiAs_2$), we first calculated the cohesive energy, defined as $E_{\text{coh}} = (nE_{\text{Si}} + mE_{\text{As}} - E_{\text{Mono}})/(n + m)$, where E_{Si}, E_{As}, and E_{Mono} are the total energies of a single Si atom, a single As atom, and one formula unit of monolayer SiAs ($SiAs_2$), respectively, and $n(m)$ is the number of As(Si) atom in the formula unit. Our calculations show that the SiAs monolayer has a cohesive energy of 5.13 eV/atom, which is a bit larger than that of $SiAs_2$ monolayer 4.98 eV/atom. For comparison, at the same theoretical level, the cohesive energies of arsenene and silicene are 2.99 and 3.71 eV/atom, respectively [18, 43]. The high cohesive energies of SiAs and $SiAs_2$ reveal that both of them are bonded strongly with high stability.

To further confirm the structural stabilities of monolayer SiAs and $SiAs_2$, we also have performed vibrational phonon spectra calculations. As shown in Fig. 2a, positive frequencies account for a majority of modes except the transverse acoustic mode near the Γ point, which is due to the softening of phonons and has been reported in other similar systems [44, 45], indicating that the structures are both dynamically stable. Then, we carried out 6 ps first-principles MD simulations at room temperature ($T = 300K$), as presented in Fig. 2b. The slight energy fluctuation and well kept sturctures suggest that they are thermally stable at room temperature. Our results imply that the monolayers SiAs and $SiAs_2$ could be realized experimental at room temperature.

With the optimized structures of monolayer SiAs and $SiAs_2$, now we pay attention to their electronic properties. The calculated orbital decomposition band structures of SiAs and $SiAs_2$ monolayers are shown in Fig. 3. Our calculations clearly show that SiAs and $SiAs_2$ monolayers are both indirect semiconductors with wide band gaps. For monolayer SiAs, the valence band maximum (VBM) is located at the Y point, while the conduction band minimum (CBM) is at the Γ (Fig. 3a). The indirect band gap of monolayer SiAs is $E_g = 1.72$ eV within the PBE scheme. One can also see that the VBM state at Y point comprises the p_y orbital, while the CBM of Γ point comprises mainly

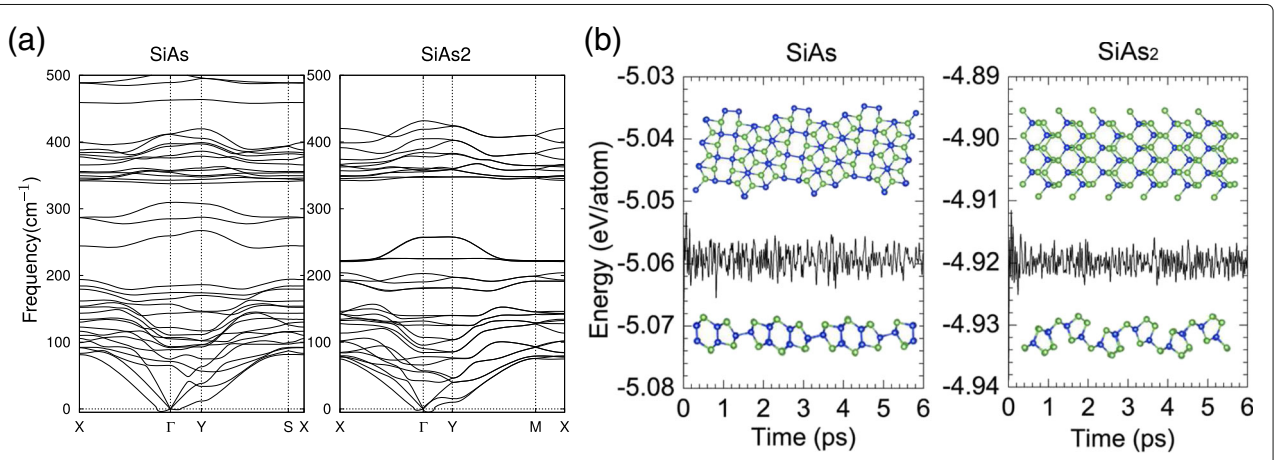

Fig. 2 Phonon dispersion curves and MD simulations of monolayers SiAs and $SiAs_2$. **a** The phonon dispersion curves for monolayer SiAs and $SiAs_2$. **b** Relationships of total energy and time during room-temperature MD simulations of SiAs and $SiAs_2$. Selected snapshots of the monolayer structures at the end of 6 ps are also provided

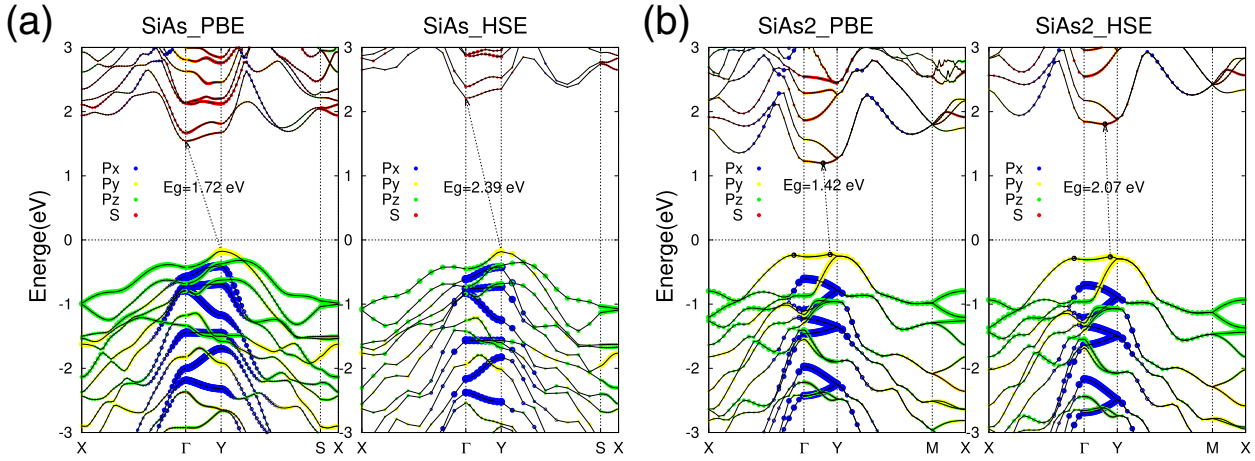

Fig. 3 Band structures of monolayer SiAs and $SiAs_2$ calculated by PBE and HSE06. The electronic orbital decomposition of band structures of monolayers SiAs and $SiAs_2$ are represented as **a** and **b**, respectively. The red dots denote *s* orbital, while blue, yellow, and green are p_x, p_y, and p_z, respectively. The Fermi level is set as zero and indicated with a dot line

the *s* orbital, which means that the external deformation will have different effects on the two states and may lead to indirect–direct transition, as revealed in the following. Unlike SiAs, the monolayer $SiAs_2$ is a nearly direct semiconductor with VBM located at side of the Y point and CBM is of a little displacement from it (Fig. 3b). The $SiAs_2$ monolayer indirect band gap is $E_g = 1.42$ eV within the PBE scheme. And the VBM and CBM of $SiAs_2$ monolayer are comprised of the p_y orbital and *s* orbital, respectively. In order to get more accurate band gap value, we also performed the hybrid functional calculations (HSE06) [46, 47] for SiAs and $SiAs_2$ monolayers. From the calculated band structures (the right part of Fig. 3a, b), the sharps of band states from PBE and HSE are basically the same, and the indirect band gap is still predicted within the hybrid functional calculations, but the gap value is increased to 2.39 eV and 2.07 eV for SiAs and $SiAs_2$, respectively.

The carrier mobilities, which is a key factor of the potential applications in modern electronic devices for the newly discovered 2D materials, is as important as the bandgap and location of CBM and VBM. To gain more details on the electronic structure properties of SiAs and $SiAs_2$ monolayers, we then calculated their acoustic phonon-limited carrier mobilities (including electron and hole in both x and y directions) on the basis of deformation potential (DP) theory [48] at the room temperature ($T = 300\ K$). At the low-energy regime ($300\ K$), the electron-acoustic-phonon scattering dominates the carrier transport, which makes the acoustic phonon-limited an effective way to predict the carrier mobilities of many 2D structures, such as the MoS_2 monolayer [49], tellurene [19], phosphene [50], and few-layer MoO_3 [51]. The calculated effective masses m^* and carrier mobilities μ of SiAs and $SiAs_2$ monolayers show that both of them are high-mobility and transport anisotropy (see Additional file 1: Table S1 and the Figures S3 and S4) like the black phosphorene [50]. To estimate the carrier mobility of SiAs and $SiAs_2$, we firstly performed a fit of their bands using the nearly free electron model to get the effective carrier masses. For SiAs, we define x and y as the direction perpendicular to the lattice vectors b and a, respectively. The m_e^* and m_h^* along the x direction are about 0.15 m_0 and 0.86 m_0, respectively, and along the y direction are 0.80 m_0 and 0.22 m_0 (m_0 is the free-electron mass), respectively. For $SiAs_2$, the direction of lattice vector a is defined as x, while that of b is y. The m_e^* and m_h^* along the x direction are about 0.14 m_0 and 0.65 m_0, respectively, and along the y direction are 2.05 m_0 and 1.82 m_0, respectively. We further studied the elastic constants (C) and the deformation potentials (E1) (see Additional file 1: Figure S2 and S3). Based on the above obtained m^*, C and E1 values, we estimated the carrier mobility as listed in Table 1. The electron mobilities for SiAs($SiAs_2$) along x and y directions are 0.66(0.26) and

Table 1 Effective masses m^* and carrier mobilities μ of SiAs and $SiAs_2$, obtained using the PBE calculation at $T = 300$K

	m^* (m_e)		μ (10^3 cm^{2}V$^{-1}s^{-1}$)	
	Electron	Hole	Electron	Hole
SiAs	0.15 (x)	0.86 (x)	0.66 (x)	3.90 (x)
	0.80 (y)	0.22 (y)	0.54 (y)	0.30 (y)
$SiAs_2$	0.14 (x)	0.65 (x)	0.26 (x)	0.13 (x)
	2.05 (y)	1.82 (y)	0.11 (y)	0.65 (y)

$0.54(0.11) \times 10^3 \cdot cm^2V^{-1}S^{-1}$, while the hole mobilities along x and y directions are 3.90(0.13) and 0.30(0.65) $\times 10^3 \cdot cm^2V^{-1}S^{-1}$, respectively, both of which are much higher than those of MoS_2 [49].

To further shed light on the underlying bonding mechanism of Si and As atoms in monolayers SiAs and $SiAs_2$, the total and partial density of states (PDOS) of them using PBE functional, with their electron density distribution corresponding to VBM and CBM, are provided in Fig. 4, respectively. One can see that the PDOS of As and Si atoms (Fig. 4a, c) shows strong hybridization of s and p orbitals , indicating the strong covalent bond between them. The distinctions between monolayers SiAs and $SiAs_2$ are the localization of p_z orbital, which are attribute to the different bonding coordination environment of As atom. The lone pair electron states, localized at As atom in both of SiAs and $SiAs_2$ monolayers, augment the three nearest bonding orbitals to decide the monolayer structure buckling formation and to form the p_z orbital localizing action. In monolayer SiAs, the lone pairs are apart by Si–As bond, which relax the repulsive effect and broaden the p_z orbital. Whereas in monolayer $SiAs_2$, As–As bond, remaining the situation which is very common in group V semiconductors, localizes the p_z orbital in a deeper energy level.

As we know, the character of frontier states is not only of interest in a microscopic understanding of the conduction channels but also of great concern for the design of optimal contacts.[52] The charge densities corresponding to VBM and CBM of monolayers SiAs and $SiAs_2$ are presented in Fig. 4b and d, respectively. The VBM is almost the hybridization of 3p orbitals of Si and As, while CBM is mainly from the contribution of 3s orbitals of Si and As, which are also consistent with PDOS results in Fig. 4a, c and the electronic orbital decomposition of band structures in Fig. 3.

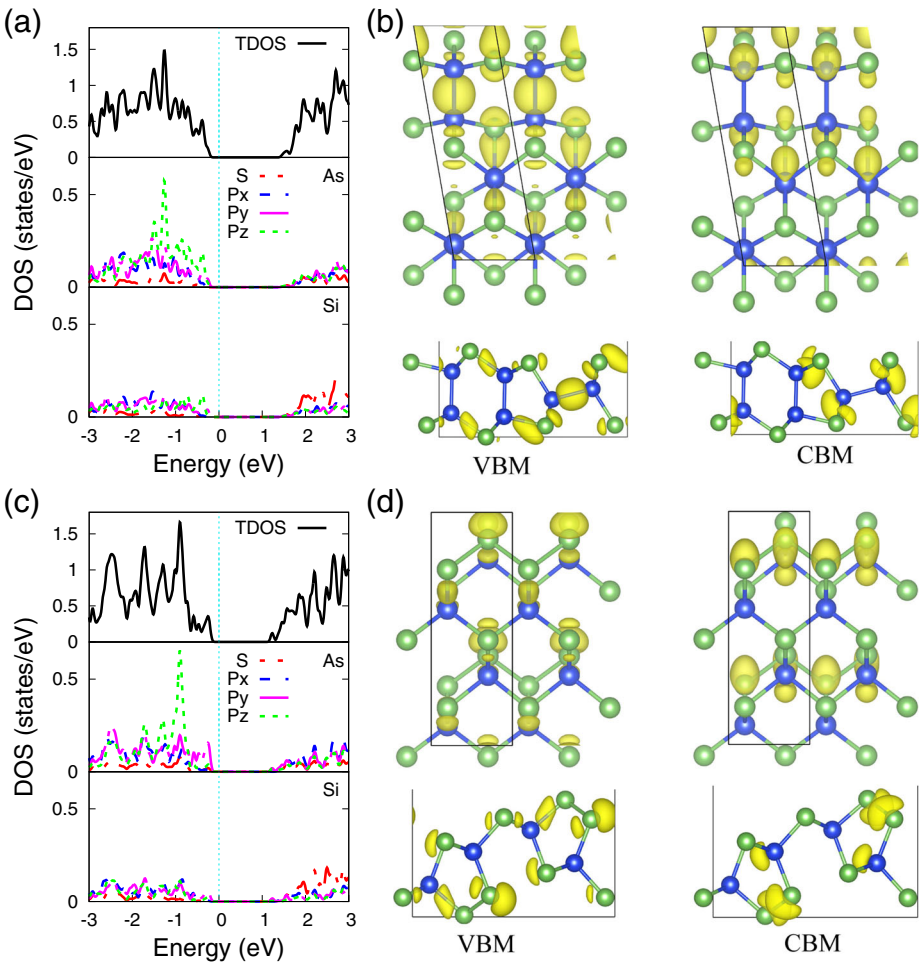

Fig. 4 Projected density of states and VBM and CBM's electron density. The projected density of states (PDOS) of As and Si atoms and the electron density distribution corresponding to VBM and CBM of (**a**, **b**) SiAs and (**c**, **d**) $SiAs_2$ monolayers. The isosurface value 0.034 $e/Å^3$

Mechanical strain is an effective way to modulate the electronic properties of 2D materials, which are extensively used to modify the band structure of black and blue phosphorenes and other nanosheet materials [53–55]. Especially, for the buckled structure system, the energy cost is usually quite small to induce a marked strain. Here, the application of mechanical strain is simulated by varying the lattice constant as well as the internal degrees of freedom of each atom during the geometric optimization. The strain ε is defined as $\varepsilon = (l - l_0)/l_0$, where l and l_0 are the strained and equilibrium lattice constants of monolayers SiAs and $SiAs_2$. In Fig. 5a, b, the detailed variations of high buckling geometric structure of 2D SiAs and $SiAs_2$ under strains are represented, respectively. One can see that their buckled heights are expanded or compressed by changed the buckled angle $\theta_{1(2)}$ with biaxial compressive or tensile strains in nearly linear variations. And we also found that their high buckling geometric structure are both still kept well under quite large strains, whose phonon spectra, as shown in Additional file 1: Figure S5 and S6, exists no negative frequencies even at the large strain regime. The gap variations of monolayer SiAs and $SiAs_2$ under biaxial compressive and tensile strains are shown in Fig. 5c, d, respectively. One can see that the electronic properties of SiAs and $SiAs_2$ sensitively depend on the strain and undergo an indirect to direct band transition in certain strain region and then to metal at a large strain region.

The detailed variations of SiAs and $SiAs_2$ band structures are exhibited in Figs. 6 and 7, respectively. Under biaxial compressive strains, the buckled height of monolayer SiAs is increasing and the CBM shifts from Γ to a point on the Y–S line and back to Y. While the VBM is kept still at Y point until the compressive strain reaches $\varepsilon = -10\%$. Therefore, with increasing compressive strain the band gap switches from indirect Y to Γ, via indirect Y to a point on the Y–S line, to direct Y to Y and back to indirect a point on the Γ–Y line to Y, as shown in Fig. 6. For tensile strains, the VBM at Y moves to a point on

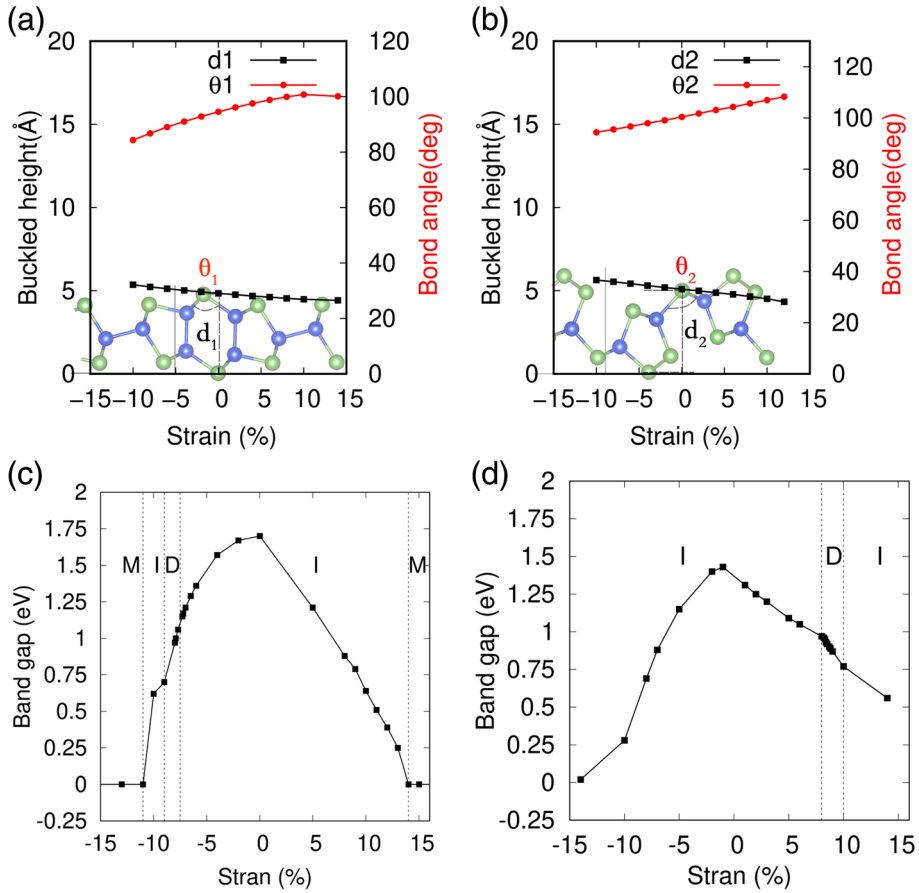

Fig. 5 Strain effects on the geometric structures and band gaps of 2D SiAs and $SiAs_2$. **a**, **c** represent SiAs; and **b**, **d** denote $SiAs_2$; M, I, and D represent metal, indirect semiconductor, and direct semiconductor, respectively

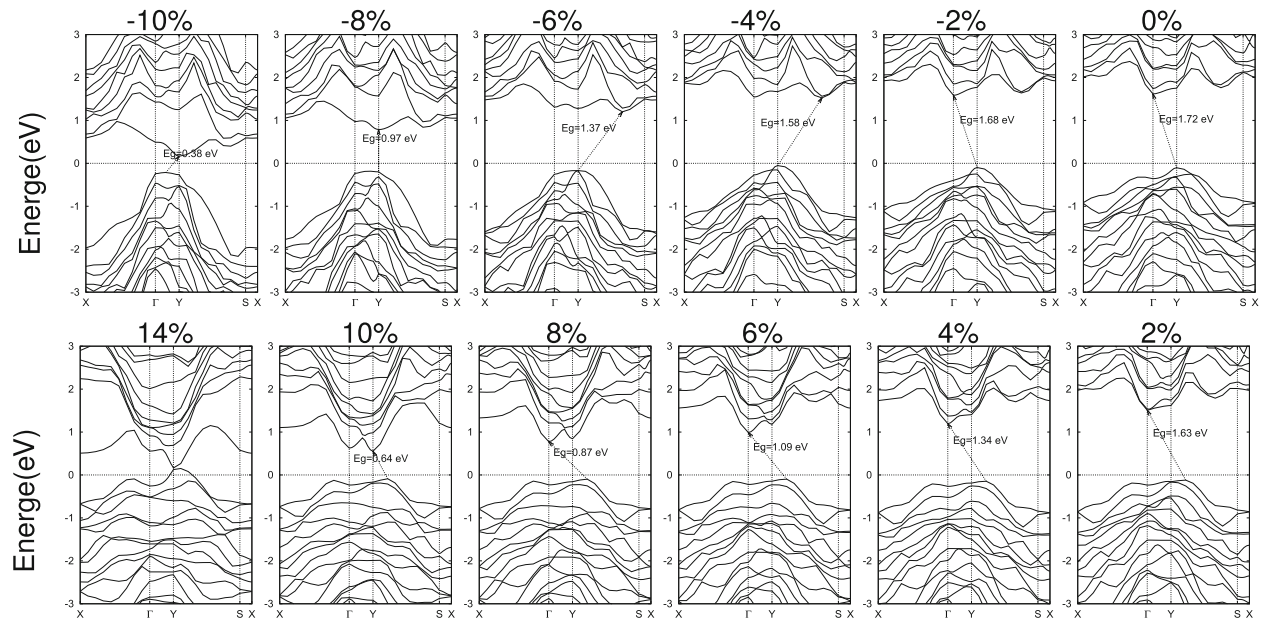

Fig. 6 Band structures of 2D SiAs under the biaxial strains. The Fermi level is set as zero and indicated with a dot line

the Y–S line and the CBM at Γ moves to Y and the band gap remains indirect. For large strain, no matter compressive or tensile leads to a metal transition, as shown in the Fig. 5c.

In Fig. 7, a similar study has been carried out for 2D $SiAs_2$. Instead of compression, tensile strains in the range of 8–10% result in direct band gaps. when the monolayer $SiAs_2$ spreads with a decreasing of buckled height under the tensile strains, the VBM shift from a point on the Γ–Y line to Γ and keep still in the range of 8–10% and then shift apart to a point on the Γ–X line, while the CBM moves from a point on the Γ–Y line to Γ and hold on. Therefore, with rising tensile strain, the band gap switches from indirect on the Γ–Y line to direct Γ–Γ and then back to indirect a point on the Γ–X line to Γ, as illustrated in Fig. 7. Compressive strains remain the indirect band gap. And large strains have similar effects, leading to a metal transition as SiAs.

Representative direct band structures of strained SiAs and $SiAs_2$ are also shown in Additional file 1: Figure S7a

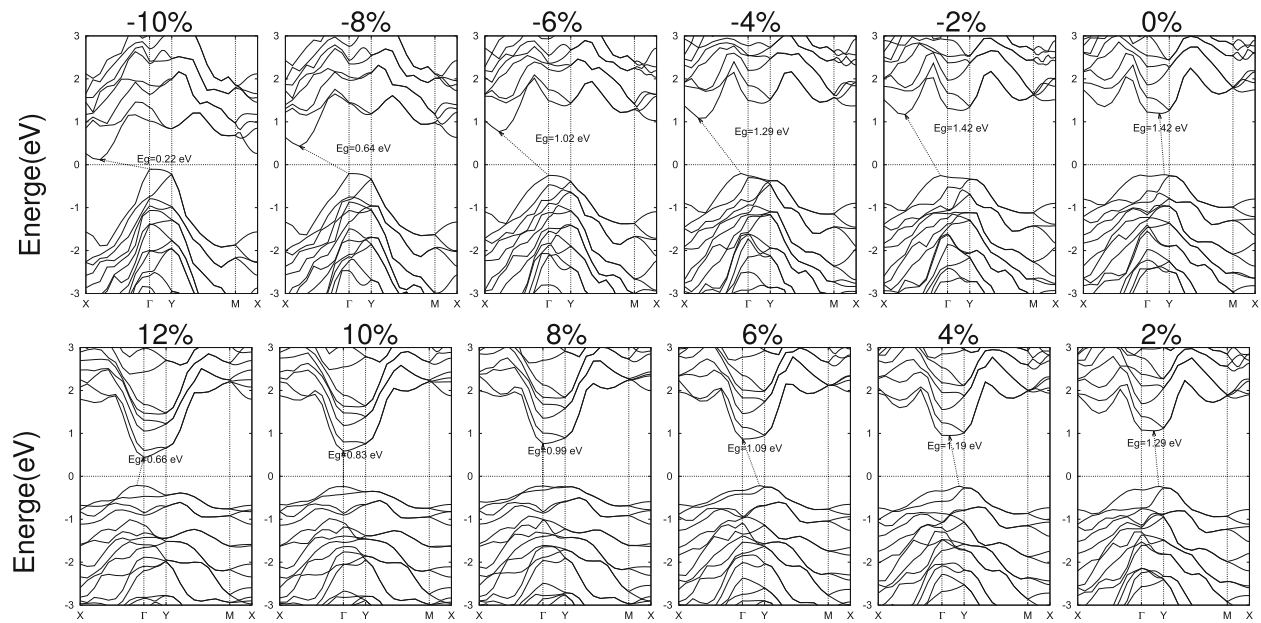

Fig. 7 Band structures of 2D $SiAs_2$ under the biaxial strains. The Fermi level is set as zero and indicated with a dot line

and b by the PBE and HSE calculations. For SiAs, a direct band gap of $E_g = 1.75\,eV$(HSE) with the VBM and CBM localized at the Y points is obtained under a biaxial compressive strain of $\varepsilon = -7.5\%$. Unlike SiAs, a biaxial tensile strains of $\varepsilon = 8.5\%$ induces the $SiAs_2$ to a direct band of $E_g = 1.60\,eV$(HSE). And the VBM and CBM are at the Γ point.

Conclusions

In summary, performing a first-principles DFT calculation, we have propsed two new kinds of 2D materials of silicon and arsenic compound, SiAs and $SiAs_2$, which are both dynamically and thermodynamically stable. Our caculations show that SiAs and $SiAs_2$ monolayers are indirect semiconductors with the band gaps of 2.39 eV and 2.07 eV, respectively. The band gap of SiAs and $SiAs_2$ monolayers are sensitive to strain, which undergo an indirect to direct band transition and even to metal upon certain mechanical strain. SiAs and $SiAs_2$ monolayers possess higher mobility than MoS_2 and display anisotropic transportation like the black phosphorene. Our works pave a new route at nanoscale for novel functionalities of optical devies.

Additional file

Additional file 1: Supplementary online material for "Strain tunable bandgap and high carrier mobility in SiAs, $SiAs_2$ monolayers from first-principles studies". (PDF 1507 kb)

Abbreviations

2D: Two-dimensional; CASTEP: Cambridge sequential total energy package; CBM: Conduction band minimum; DFT: Density functional theory; DFPT: Density functional perturbation theory; DP: Deformation potential; GGA: Generalized gradient approximation; MD: Molecular dynamics; NVT: Moles-volume-temperature; PAW: Projector augmented wave; PBE: Perdew-Burke-Ernzerhof; PDOS: Partial density of states; TMDs: Transiton-metal dichalcogenides; VASP: Vienna ab initio simulation package; VBM: Valence band maximum

Acknowledgements

This work was supported by the National Natural Science Foundation of China (nos. 11504332 and 11774078) and Innovation Scientists and Technicians Troop Construction Projects of Henan Province (no. 10094100510025) and the key Research Project for the Universities of Henan Province (19A140009) and Doctoral Foundation of Henan Polytechnic University (B2018-38). The calculations were performed on the High Performance Computational Center of Zhengzhou University.

Availability of Data and Materials

All data generated or analyzed during this study are included in this published article.

Authors' Contributions

YJ and CYN conceived the idea. SYB performed the calculations, analyzed the result data, and wrote the manuscript. All authors have read and approved the final manuscript.

Competing Interests

The authors declare that they have no competing interests.

Publisher's Note

Received: 13 August 2018 Accepted: 19 November 2018
Published online: 12 December 2018

References

1. Berger C, Song Z, Li X, Wu X, Brown N, Naud C, Mayou D, Li T, Hass J, Marchenkov AN, et al (2006) Electronic confinement and coherence in patterned epitaxial graphene. Science 312(5777):1191–1196
2. Novoselov KS, Geim AK, Morozov SV, Jiang D, Zhang Y, Dubonos SV, Grigorieva IV, Firsov AA (2004) Electric field effect in atomically thin carbon films. Science 306(5696):666–669
3. Castro Neto AH, Guinea F, Peres NMR, Novoselov KS, Geim AK (2009) The electronic properties of graphene. Rev Mod Phys 81:109–162
4. Li X, Cai W, An J, Kim S, Nah J, Yang D, Piner R, Velamakanni A, Jung I, Tutuc E (2009) Others: Large-area synthesis of high-quality and uniform graphene films on copper foils. Science 324(5932):1312–1314
5. Vogt P, De Padova P, Quaresima C, Avila J, Frantzeskakis E, Asensio MC, Resta A, Ealet B, Le Lay G (2012) Silicene: compelling experimental evidence for graphenelike two-dimensional silicon. Phys Rev Lett 108(15):155501
6. Fleurence A, Friedlein R, Ozaki T, Kawai H, Wang Y, Yamada-Takamura Y (2012) Experimental evidence for epitaxial silicene on diboride thin films. Phys Rev Lett 108(24):245501
7. Zhang WB, Song ZB, Dou LM (2015) The tunable electronic structure and mechanical properties of halogenated silicene: a first-principles study. J Mater Chem C 3(13):3087–3094
8. Chopra NG, Luyken RJ, Cherrey K, Crespi VH, Cohen ML, Louie SG, Zettl A (1995) Boron nitride nanotubes. Science 269(5226):966–967
9. Dean CR, Young AF, Meric I, Lee C, Wang L, Sorgenfrei S, Watanabe K, Taniguchi T, Kim P, Shepard KL, et al. (2010) Boron nitride substrates for high-quality graphene electronics. Nat Nanotechnol 5(10):722
10. Wang QH, Kalantar-Zadeh K, Kis A, Coleman JN, Strano MS (2012) Electronics and optoelectronics of two-dimensional transition metal dichalcogenides. Nat Nanotechnol 7(11):699
11. Wilson JA, Yoffe AD (1969) The transition metal dichalcogenides discussion and interpretation of the observed optical, electrical and structural properties. Adv Phys 18(73):193–335
12. Li L, Yu Y, Ye GJ, Ge Q, Ou X, Wu H, Feng D, Chen XH, Zhang Y (2014) Black phosphorus field-effect transistors. Nat Nanotechnol 9(5):372
13. Liu H, Neal AT, Zhu Z, Luo Z, Xu X, Tománek D, Ye PD (2014) Phosphorene: an unexplored 2d semiconductor with a high hole mobility. ACS Nano 8(4):4033–4041
14. Li WL, Chen Q, Tian WJ, Bai H, Zhao YF, Hu HS, Li J, Zhai HJ, Li SD, Wang LS (2014) The B35 cluster with a double-hexagonal vacancy: a new and more flexible structural motif for borophene. J Am Chem Soc 136(35):12257–12260
15. Jiang HR, Lu Z, Wu MC, Ciucci F, Zhao TS (2016) Borophene: a promising anode material offering high specific capacity and high rate capability for lithium-ion batteries. Nano Energy 23:97–104
16. Peng B, Zhang H, Shao H, Xu Y, Zhang R, Zhu H (2016) The electronic, optical, and thermodynamic properties of borophene from first-principles calculations. J Mater Chem C 4(16):3592–3598
17. Zhang S, Yan Z, Li Y, Chen Z, Zeng H (2015) Atomically thin arsenene and antimonene: semimetal–semiconductor and indirect–direct band-gap transitions. Angew Chemie 127(10):3155–3158
18. Kamal C, Ezawa M (2015) Arsenene: Two-dimensional buckled and puckered honeycomb arsenic systems. Phys Rev B 91(8):85423
19. Zhu Z, Cai X, Yi S, Chen J, Dai Y, Niu C, Guo Z, Xie M, Liu F, Cho JH (2017) Others:Multivalency-driven formation of Te-based monolayer materials: a combined first-principles and experimental study. Phys Rev Lett 119(10):106101
20. Zhu Z, Guan J, Liu D, Tománek D (2015) Designing Isoelectronic Counterparts to Layered Group V Semiconductors. ACS Nano 9(8):8284–8290
21. Guan J, Liu D, Zhu Z, Tománek D (2016) Two-dimensional phosphorus carbide: Competition between sp2 and sp3 bonding. Nano Lett 16(5):3247–3252

22. Zhang S, Guo S, Huang Y, Zhu Z, Cai B, Xie M, Zhou W, Zeng H (2016) Two-dimensional SiP: an unexplored direct band-gap semiconductor. 2D Mater 4(1):015030
23. Zhang WB, Qu Q, Zhu P, Lam CH (2015) Robust intrinsic ferromagnetism and half semiconductivity in stable two-dimensional single-layer chromium trihalides. J Mater Chem C 3(48):12457–12468
24. Elias DC, Nair RR, Mohiuddin TMG, Morozov SV, Blake P, Halsall MP, Ferrari AC, Boukhvalov DW, Katsnelson MI, Geim AK, et al. (2009) Control of graphene's properties by reversible hydrogenation: evidence for graphane. Science 323(5914):610–613
25. Han MY, Özyilmaz B, Zhang Y, Kim P (2007) Energy band-gap engineering of graphene nanoribbons. Phys Rev Lett 98(20):206805
26. Radisavljevic B, Radenovic A, Brivio J, Giacometti IV, Kis A (2011) Single-layer MoS2 transistors. Nat Nanotechnol 6(3):147
27. Fuhrer MS, Hone J (2013) Measurement of mobility in dual-gated MoS2 transistors. Nat Nanotechnol 8(3):146
28. Weck PF, Kim E, Czerwinski KR (2013) Semiconducting layered technetium dichalcogenides: insights from first-principles. Dalt Trans 42(43):15288–15295
29. Wood JD, Wells SA, Jariwala D, Chen KS, Cho E, Sangwan VK, Liu X, Lauhon LJ, Marks TJ, Hersam MC (2014) Effective passivation of exfoliated black phosphorus transistors against ambient degradation. Nano Lett 14(12):6964–6970
30. Barreteau C, Michon B, Besnard C, Giannini E (2016) High-pressure melt growth and transport properties of SiP, SiAs, GeP, and GeAs 2D layered semiconductors. J Cryst Growth 443:75–80
31. Wadsten T, Vikan M, Krohn C, Åke Nilsson, Theorell H, Blinc R, Paušak S, Ehrenberg L, Dumanović J (1967) The Crystal Structures of SiP2, SiAs2, and GeP. Acta Chem Scand 21(21):593–594
32. Donohue P, Siemons W, Gillson J (1968) Preparation and properties of pyrite-type SiP2 and SiAs2. J Phys Chem Solids 29(5):807–813
33. Kresse G, Furthmüller J (1996) Efficient iterative schemes for ab initio total-energy calculations using a plane-wave basis set. Phys Rev B 54(16):11169
34. Perdew JP, Burke K, Ernzerhof M (1996) Generalized gradient approximation made simple. Phys Rev Lett 77(18):3865
35. Kresse G, Joubert D (1999) From ultrasoft pseudopotentials to the projector augmented-wave method. Phys Rev B 59(3):1758
36. Monkhorst HJ, Pack JD (1976) Special points for Brillouin-zone integrations. Phys Rev B 13(12):5188
37. Togo A, Oba F, Tanaka I (2008) First-principles calculations of the ferroelastic transition between rutile-type and CaCl 2-type SiO 2 at high pressures. Phys Rev B 78(13):134106
38. Togo A. https://atztogo.github.io/phonopy/
39. Clark SJ, Segall MD, Pickard CJ, Hasnip PJ, Probert MJ, Refson K, Payne MC (2005) First principles methods using CASTEP. Z Kristall 220:567–570
40. Refson K, Tulip PR, Clark SJ (2006) Variational density-functional perturbation theory for dielectrics and lattice dynamics. Phys Rev B 73:155114
41. Porezag DV, Pederson MR (1996) Infrared intensities and raman-scattering activities within density-functional theory. Phys Rev B 54:7830–7836
42. Molina-Sánchez A, Wirtz L (2011) Phonons in single-layer and few-layer mos_2 and ws_2. Phys Rev B 84:155413
43. Li Y, Liao Y, Chen Z (2014) Be2C Monolayer with quasi-planar hexacoordinate carbons: a global minimum structure. Angew Chemie Int Ed 53(28):7248–7252
44. Zheng H, Li XB, Chen NK, Xie SY, Tian WQ, Chen Y, Xia H, Zhang SB, Sun HB (2015) Monolayer ii-vi semiconductors: A first-principles prediction. Phys Rev B 92:115307
45. Şahin H, Cahangirov S, Topsakal M, Bekaroglu E, Akturk E, Senger RT, Ciraci S (2009) Monolayer honeycomb structures of group-iv elements and iii-v binary compounds: First-principles calculations. Phys Rev B 80:155453
46. Heyd J, Scuseria GE, Ernzerhof M (2003) Hybrid functionals based on a screened Coulomb potential. J Chem Phys 118(18):8207–8215
47. Krukau AV, Vydrov OA, Izmaylov AF, Scuseria GE (2006) Influence of the exchange screening parameter on the performance of screened hybrid functionals. J Chem Phys 125(22):224106
48. Bardeen J, Shockley W (1950) Deformation potentials and mobilities in non-polar crystals. Phys Rev 80(1):72
49. Kaasbjerg K, Thygesen KS, Jacobsen KW (2012) Phonon-limited mobility in n-type single-layer mos_2 from first principles. Phys Rev B 85:115317
50. Qiao J, Kong X, Hu ZX, Yang F, Ji W (2014) High-mobility transport anisotropy and linear dichroism in few-layer black phosphorus. Nat Commun 5:4475
51. Zhang WB, Qu Q, Lai K (2017) High-mobility transport anisotropy in few-layer MoO3 and its origin,. Acs Appl Mater Interfaces 9(2):1702–1709
52. Tománek D (2015) Interfacing graphene and related 2D materials with the 3D world. J Phys Condens Matter 27(13):133203
53. Peng X, Wei Q, Copple A (2014) Strain-engineered direct-indirect band gap transition and its mechanism in two-dimensional phosphorene. Phys Rev B 90(8):85402
54. Fei R, Yang L (2014) Strain-engineering the anisotropic electrical conductance of few-layer black phosphorus. Nano Lett 14(5):2884–2889
55. Yu W, Niu CY, Zhu Z, Wang X, Zhang WB (2016) Atomically thin binary V-V compound semiconductor: a first-principles study. J Mater Chem C 4(27):6581–6587